

Discovery of knowledge of wall-bounded turbulence via symbolic regression

ZhongXin Yang^a, XiangLin Shan^a, and WeiWei Zhang^a

^aNorthwestern Polytechnical University, Xi'an 710072, China

May 2024

Abstract

With the development of high performance computer and experimental technology, the study of turbulence has accumulated a large number of high fidelity data. However, few general turbulence knowledge has been found from the data. So we use the symbolic regression (SR) method to find a new mixing length formula which is generally valid in wall-bounded turbulence, and this formula has physical interpretation that it has correct asymptotic relationships in viscous sublayer,buffer layer, log-law region and outer region. Coupled with Reynolds averaged Navier-Stokes (RANS) solver, we test several classic cases. The prediction results fully demonstrate the accuracy and generalization of the formula. So far, we have found that SR method can help us find general laws from complex turbulent systems, and it is expected that through this 'white box' machine learning method, more turbulence knowledge with physical interpretation can be found in the future.

1 Introduction

From ancient to modern, the main ways to conduct scientific research have gradually changed. First, Humanity's earliest scientific research, characterized primarily by the recording and description of natural phenomena, is called experimental science(the first paradigm), such as the famous Reynolds experiment. However, due to the limitations of experimental conditions, it is difficult to achieve a more accurate understanding of nature, so theoretical science (the second paradigm) is emerged which through theoretical simplification, leaves only the key factors for research. A successful example is the Reynolds averaged Navier-Stokes (RANS) equation [Reynolds, 1895]. Later, with the birth of electronic computers, it became possible to solve partial differential equations (PDEs), so numerical simulation (the third paradigm) was born. During this period, the development speed of human beings was significantly improved, and many disciplines were derived, such as computational fluid mechanics [Anderson and Wendt, 1995]. With the further development of computer, the data is expected to explode from 33 zettabytes in 2018 to 175 zettabytes in 2025. Then data-intensive sciences [Hey et al., 2009] comes into public view. This approach to science is known as the fourth paradigm. With the help of Artificial Intelligence (AI), a lot of research in fluid dynamics has been conducted. In the aspect of flow control,Yu Zhou et al [Zhou et al., 2020]proposed an artificial intelligence control system to maximize the mixing rate of turbulent jets. In terms of mode reduction,Murata et al. [Murata et al., 2020] proposed a nonlinear mode decomposition method for flow field based on convolutional neural networks, which has good feature separation potential compared with Proper Orthogonal Decomposition method. In the area of turbulence modeling ,Dehao Xu et al. proposed a nonlinear algebraic model based on neural networks for large eddy simulation (LES) of compressible wall turbulence [Xu et al., 2023]. Park et al. proposed a neural network-based SubGrid-Scale model (SGS) for incompressible channel turbulent flow [Park and Choi, 2021].

Many of the above are examples of using data for fluid dynamics research, and the fundamental logic of using big data analysis for scientific research is that the generation of data necessarily contains knowledge [Cheng et al., 2018]. The function of AI is to replace people to mine this law in massive data. There is already a lot of work combining AI with fluid mechanics. Julia Ling et al. [Ling et al., 2016] proposed a neural network that satisfies Galilean invariance and obtained better results than naive neural networks without embedded invariance. Zhu et al. [Zhu et al., 2021] and Shan et al. [Shan et al., 2023]directly constructed a turbulence model using deep neural networks and achieved good results on airfoil flow. But the shortcoming is that this method is difficult to have no reasonably physical explanation. Peng Cui et al. [Cui and Athey, 2022]pointed out that physical interpretability is a key problem to be solved in machine learning at present. Due to the high complexity of many application areas,

machine learning models struggle to explain algorithmic processes and predictive results to humans. However, in areas such as health care, financial justice, etc., the potential risk of incorrect predictions due to the lack of physical explanation can bring great harm and is an urgent problem in the field of machine learning. The symbolic regression has the characteristic of good physical interpretation. Symbolic regression works by finding an analytic parameterized function that best describes the given data [de França et al., 2023]. It has been applied to materials science [Wang et al., 2019], astrophysics [Matchev et al., 2022, Wadekar et al., 2023]. And it has been gradually applied in the field of fluid mechanics. Jun Zhang et al. [Zhang and Ma, 2020] used the sparse recognition method to obtain the correct form of the governing equation from the data simulated by the molecule and accurately determine the value of the transport coefficient. Wu Chengyu et al. [Wu and Zhang, 2023] modified the generation term coefficient of the SST turbulence model by using the symbolic regression method to enhance the prediction accuracy of the SST model in separated flows. The essence of the success of these works is that the development of things follows the objective physical laws, and the knowledge is hidden in the observation data. How to discover knowledge from the data has become a new research paradigm!

In this paper, we used SR method for the first time to mine a physically interpretable mixing-length formula from high-fidelity data, and calculate several cases coupled with RANS solver. Therefore, the accuracy and generalization of the mixing-length formula are fully tested. The prediction results show that the formula is more accurate, compared with the traditional turbulence model in practical calculation.

The rest of the paper is organised as follows. The symbolic regression procedure and formula discovered are described in Part 2. The interpretability of the formula is given in Part 3. The assessment of the formula under the RANS framework is shown in Part 4. Finally, conclusions are given in Part 5.

2 Discovery of a new Mixing-Length formula

Despite its simplicity, Prandtl's mixing-length hypothesis [Prandtl, 1925] is still a cornerstone of our understanding of wall-bounded turbulence. Prandtl says that l 'may be considered as the diameter of the masses of fluid moving as a whole in each individual case; or again, as the distance traversed by a mass of the type before it becomes blended in with neighbouring masses...'; and also that l is 'somewhat similar, as regards effect, to the mean free path in the kinetic theory of gases'. Pirozzoli [Pirozzoli, 2014] also suggested close connection between the mixing length and the physical size of the outer-layer eddies.

Under the boussinesq eddy hypothesis, the Reynolds stress and mean velocity gradient have a relationship as follows:

$$-\overline{u'v'} = \nu_T \frac{\partial \bar{u}}{\partial y} \quad (1)$$

where $-\overline{u'v'}$ is Reynolds stress, ν_T is eddy viscosity and $\frac{\partial \bar{u}}{\partial y}$ is mean velocity gradient. To describe the eddy viscosity, a mixing length, l , is introduced here.

$$\nu_T = l^2 \left| \frac{\partial \bar{u}}{\partial y} \right| \quad (2)$$

In any turbulence boundary layer flow, the mixing length can be computed from measured profiles of velocity and shear stress.

$$l^2 = \frac{-\overline{u'v'}}{\partial \bar{u} / \partial y} \quad (3)$$

Next, symbolic regression (SR) method will be introduced. Like fully connected neural network, SR is also a machine learning method. But different from the former, it can get an explicit mathematical expression, which can be explained. So it's called 'White box' model, while neural network is named 'black box'. In this paper, we use a symbolic regression method from a third party python library called PySR [Cranmer, 2023].

In this section, the different physical factors (e.g., intermittent, pressure gradient) are broken down into multiple steps for regression to ensure that the effects of different physical factors will not be confused by machine learning, and also to help improve the accuracy of the formula. In the first step, the basic mixing length relationship will be discovered from the fully developed channel flow; The second step is to find the outer region characteristics of mixing length according to the intermittent characteristics of turbulence in boundary layer flow. In the third step, considering the influence of adverse pressure gradient, the mixing length formula is modified by pressure gradient correction parameter (γ). This strategy is called the three-step strategy

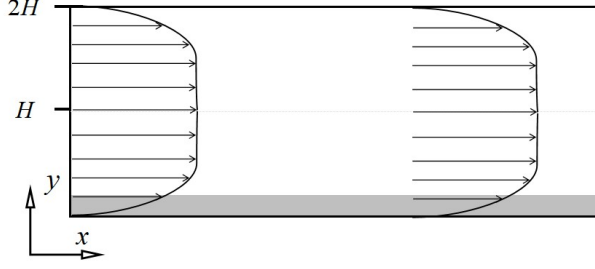


Figure 1: Channel flow

2.1 Step1

Fully developed channel flow is shown in Fig.1. The simulations reported here are DNS of incompressible turbulent flow between two parallel planes. Periodic boundary conditions are applied in the streamwise (x) and spanwise (z) directions, and no-slip/no-penetration boundary conditions are applied at the wall. The computational domain sizes are $L_x = 8\pi H$ and $L_z = 3\pi H$, where H is the channel half-width, so the domain size in the wall-normal (y) direction is 2H. The flow is driven by a uniform pressure gradient.

The DNS was carried out by Myoungkyu Lee et al. [Lee and Moser, 2015] And in step 1, the DNS data will be used to compute the mixing length, according to Eq.(3). The channel data of the grey part at two friction Reynolds numbers Re_τ ($Re_\tau = \frac{H u_\tau}{\nu}$) are used as training set, while the data of the other three friction Reynolds numbers will be used to test the generalization ability of the formula, as shown in Table 1.

Re_τ	Property
180	test
550	test
1000	train
2000	test
5200	train

Table 1: Channel flow data

In the first step, five dimensionless variables are given as input variables in Eq.(4).

$$x_0 = \frac{y}{H}, x_1 = Re_\tau, x_2 = y^+, x_3 = \sqrt{\frac{y}{H}}, x_4 = \sqrt{y^+} \quad (4)$$

where $y^+ = \frac{\sqrt{\rho\tau_w}}{\mu} y$. To reduce the difficulty of symbolic regression, the Van Driest's damping function (Eq.(5)) [Van Driest, 1956] is used to get a higher fidelity mixing length formula.

$$l = \kappa y (1 - e^{-\frac{y^+}{A^+}}) \quad (5)$$

The objective function is listed in Eq.(6).

$$y_{obj,1} = \frac{l_{hf,1}}{\kappa y (1 - e^{-\frac{y^+}{A^+}})} \quad (6)$$

where $\kappa = 0.41$, and subscript obj,1 and hf,1 represent the objective function and the mixing length computed from high fidelity (hf) data by Eq.(3) in step1 respectively.

Table.2 shows operators used in symbolic regression.

Operator Type	Operators
Unary operators	$exp(x_j), ln(x_j), tanh(x_j)$
Binary operators	$x_i + x_j, x_i * x_j, \frac{x_i}{x_j}, 1 - exp(-\frac{x_i}{x_j})$

Table 2: Operator used in SR

Loss function is defined in Eq.(7)

$$Loss_u(E) = \ln(\text{abs}(\frac{y_{predict} - y_{target}}{y_{target}}) + 1) \quad (7)$$

E denotes a generated expression by PySR, $y_{predict}, y_{target}$ represent the values predicted by E and expected values respectively. Subscript u means loss function is defined by users. In addition to the user-defined loss function, PySR adds a complexity penalty mechanism, due to the traditional philosophy of scientists, the simpler the expression is the easier to interpret by scientists. Thus, PySR allows adaptive adjustment of penalty complexity to expect that the number of expressions of different complexity are roughly equal. PySR calculates the complexity of each expression by Eq.(8).

$$C(E) = N_{var} + N_{const} + N_{op} \quad (8)$$

where $N_{var}, N_{const}, N_{op}$ denote the complexity of variables, constant and operator respectively. $C(E)$ represents the complexity of the expression E. PySR computes the complexity of each expression by Eq.(9) finally.

$$Loss(E) = Loss_u(E) * \exp(\text{frequency}[C(E)]) \quad (9)$$

where $\text{frequency}[C(E)]$ represents the ratio of expressions which have the same complexity with expression E.

Finally, combine the most reasonable expression chosen from generated expressions with with Eq.(5). The mixing length discovered is listed in Eq.(10)

$$l = \kappa y \frac{(1 - e^{-\frac{y^+}{A^+}})}{1 - e^{-\frac{\sqrt{y^+}}{3.6}} + 1.21 \frac{y^+ + \sqrt{y^+}}{e^{\sqrt{y^+}} + 8.19}} e^{-\frac{y}{H}} \quad (10)$$

After observation , Eq.(10) can be simplified as follows.

$$l = \kappa y f_{inner}(y^+) g_{outer}(\frac{y}{H}) \quad (11)$$

where $f_{inner}(y^+)$ is:

$$f_{inner}(y^+) = \frac{(1 - e^{-\frac{y^+}{A^+}})}{1 - e^{-\frac{\sqrt{y^+}}{3.6}} + 1.21 \frac{y^+ + \sqrt{y^+}}{e^{\sqrt{y^+}} + 8.19}} \quad (12)$$

$g_{outer}(\frac{y}{H})$ is:

$$g_{outer}(\frac{y}{H}) = e^{-\frac{y}{H}} \quad (13)$$

The subscript 'inner' represents that the input of Eq.(12) is inner scale y^+ , and its value is approximately 1 in the outer layer ($y^+ > 50$). On the contrary, the subscript 'outer' denotes the input of Eq.(13) is outer scale $\frac{y}{H}$, and it does not affect the inner layer ($\frac{y}{H} < 0.1$). Because its value is approximately 1 in the inner layer.

2.2 Step2

Considering that the main flow condition in the aviation is external flow, such as flow around airfoil. Unlike channel flow, there is an intermittent flow phenomenon. The actual outer edge of the turbulent boundary layer is an extremely irregular and unsteady interface. At the position near the nominal outer edge of the boundary layer (δ_{99}), the flow is turbulent for sometime and laminar for another time. This phenomenon of alternating turbulence and laminar flow at the same point in space is called intermittent phenomenon. Klebanoff [Klebanoff, 1955] tested the distribution of the intermittent factor in a turbulent boundary layer along a smooth plate, and found that the interval mainly appears outside 0.4 times the thickness of the boundary layer. Therefore, once again we consider the mixed length formula of the external flow, considering the intermittency, the outer layer function should be replaced. The new outer layer function is found from the turbulent boundary layer of a flat plate with zero pressure gradient, and the data is derived from the large eddy simulation data of Georg Eitel-Amor et al. [Eitel-Amor et al., 2014]. The simulation was carried out on a flat plate, and the transition was triggered by the tripping device. The dimensions of the physical domain in the streamwise, wall-normal, and spanwise direction are $L_x \times L_y \times L_z = 13500 \times 400 \times 540$ measured in displacement thickness at the inlet δ^* , whereas an open boundary is modelled in the wall-normal direction. Since the purpose of this step is to fine the outer layer function of the mixing length in external flow, only the data located at the outer layer ($0.2\delta_{99} \sim 0.8\delta_{99}$ exactly) is selected as the training set,

and a total of 11 sections which the friction Reynolds number ranging from 450 to 2500 are used. Below are input variables in step 2.

$$x_0 = \frac{y}{\delta_{99}}, x_1 = Re_\tau \quad (14)$$

The objective function is shown in Eq.(15).

$$y_{obj,2} = \frac{l_{hf,2}}{\kappa y f_{inner}(y^+)} \quad (15)$$

where $f_{inner}(y^+)$ is Eq.(12). Besides ,operators and loss function are the same in step1. Through this step,another outer layer function is discovered .

$$h_{outer} = \tanh(l_k(\frac{y}{\delta_{99}})^{-1}) \quad (16)$$

where δ_{99} is the thickness of boundary layer ,and l_k is a function of Re_τ .Its form is shown here.

$$l_k = 0.215 + (Re_\tau + 1.0086^{Re_\tau}) \quad (17)$$

2.3 Step3

In addition to the intermittent of boundary layer flow, the pressure gradient caused by curvature effects is also not negligible in industrial applications (e.g., wing surface curvature).Pressure gradients are ubiquitous in real flows, and their effects are elusive. At present, there is no specific theoretical framework for the boundary layer of pressure gradient to describe the influence of pressure gradient [Bobke et al., 2017, Gungor et al., 2016].To understand the boundary layer flow under pressure gradient ,Townsend [Townsend, 1956,Townsend, 1961] proposed a definition of equilibrium boundary layer,but it is extremely strict. But Townsend and Mellor&Gibson [Mellor and Gibson, 1966] proposed another similar definition named near-equilibrium boundary layer and how to satisfy near-equilibrium conditions.Near-equilibrium boundary layer should satisfy the following relation:

$$U_\infty = C(x - x_0)^m \quad (18)$$

Where C and m are constants , x_0 is the virtual origin.Townsend pointed out m should be greater than $-\frac{1}{3}$ to achieve near-equilibrium condition.Besides,Clauser [Clauser, 1956] summarized a parameter to describe pressure gradient $\beta = \frac{\delta^+}{\tau_w} \frac{dp_e}{dx}$ (δ^* is the thickness of boundary layer, τ_w is the wall shear stress, p_e is the pressure at the outer edge of the boundary layer) to quantitatively characterize the magnitude of pressure gradient.

Data used here is simulated by well resolved large eddy simulation under different adverse pressure gradient.Details can be found in ref [Bobke et al.,].Listed below are data sets for training.Here ,only inner layer where ($y^+ < 50$) are used.A pressure gradient force first influences the inner layer and then the outer layer. Additionally, the pressure gradient initially affects the mean flow, through which it influences the turbulence. Therefore, in terms of turbulence modeling, the inner layer necessitates more significant pressure gradient corrections than the outer layer. This is why we concentrate on calibrating the model within the inner layer where y^+ is less than 50.

Case	Re_θ	β	m
M16	[1010,4000]	[1.55,2.55]	-0.16
B1	[910,3360]	≈ 1	-0.14

Table 3: Adverse Pressure Gradient flat plate boundary layer flow data

Re_θ is Reynolds number range based on momentum thickness.

The input variables is listed below.

$$x_0 = y^+, x_1 = P^+ \quad (19)$$

where $P^+ = \frac{\nu}{\rho u_\tau^3} \frac{dp_e}{dx}$ is dimensionless pressure gradient. The target funtion is :

$$y_{obj,3} = \frac{l_{hf,3}}{\kappa y f_{inner}(y^+) h_{outer}(\frac{y}{\delta_{99}}, Re_\tau)} \quad (20)$$

Other setting is the same as Step1.

Finally,we discovered the function and called it by the name of γ

$$\gamma = 1 + 18P^+(1 - \tanh(\frac{y^+ - 12.7}{14})) \quad (21)$$

3 The interpretability of the formula

We summarize Eq.(11),Eq.(13),Eq.(16),Eq.(21) here.

$$l = \kappa y f_{inner}(y^+) F_{outer} \gamma \quad (22)$$

$$F_{outer} = \begin{cases} e^{-\frac{y}{\delta}} , & \text{for channel flow} \\ \tanh(l_k(\frac{y}{\delta_{99}})^{-1}), & \text{for boundary layer flow} \end{cases} \quad (23)$$

where f_{inner} is Eq.(12),and γ is Eq.(21),and l_k is Eq.(17).

A similar form was first proposed by Cebeci and Bradshaw [Cebeci and Bradshaw, 2013]. They combined Eq.([Van Driest, 1956]) with Eq.(24) resulting in Eq.(25),and found it valid for the whole pipe flow.

$$\frac{l}{R} = 0.14 - 0.08(1 - \frac{y}{R})^2 - 0.06(1 - \frac{y}{R})^4 \quad (24)$$

$$\frac{l}{R} = (0.14 - 0.08(1 - \frac{y}{R})^2 - 0.06(1 - \frac{y}{R})^4)(1 - e^{-\frac{y^+}{A^+}}) \quad (25)$$

Later , You Wu et al. [Wu et al., 2013] used a similar form in their SED-SL model. These examples can prove that the law truly exists in the data, whereas it was previously deduced through theory, but for the first time we have mined this law directly from the data.

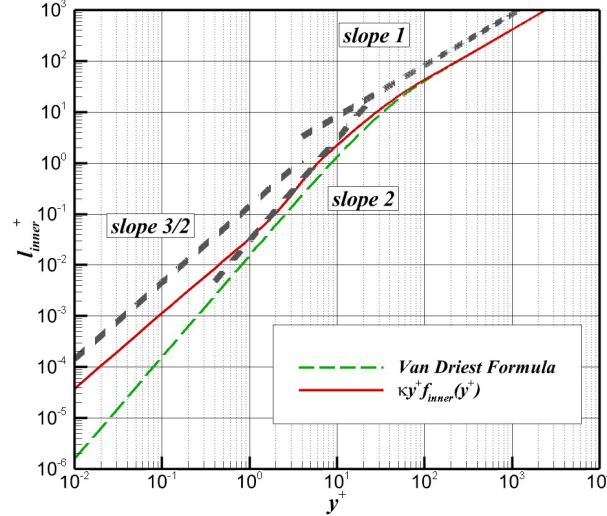


Figure 2: Asymptotic analysis chart

For a better explanation of Eq.(22) and Eq.(23),two functions will be introduced to analyze their mathematical characteristics.

$$l_{inner}^+ = \kappa y^+ f_{inner}(y^+) \quad (26)$$

$$l_{outer} = \kappa y F_{outer} \quad (27)$$

In Fig.2,it can be seen that there are three simple relationships, $l_{inner}^+ \sim y^{+\frac{3}{2}}$ in viscous sublayer, $l_{inner}^+ \sim y^{+2}$ in buffer layer, and $l_{inner}^+ \sim y^{+1}$ in low-law region respectively. $l_{inner}^+ \sim y^{+\frac{3}{2}}$ can be obtained by asymptotic analysis near the wall. The explanation of $l_{inner}^+ \sim y^{+2}$ can be referred to the work of Xi Chen et al. [Chen et al., 2018]. $l_{inner}^+ \sim y^{+1}$ is the most commonly used law of the wall(Low).

Next we show the outer region properties of the mixing length in Fig.3, where the value of l_k in Eq.(23) as a function of Re_τ is taken to be 0.215.And 0.215, as we will explain later in Fig.4, is also a specially asymptotic value at high Reynolds number.

Escudier et al. [Escudier and Spalding, 1966] and Adams et al. [Adams and Johnston, 1984] both gave the maximum values for the mixing length in boundary layer flow , 0.075 and 0.086 times the boundary layer thickness, respectively, and it is found that Adams's results have significantly higher accuracy by our modern symbolic

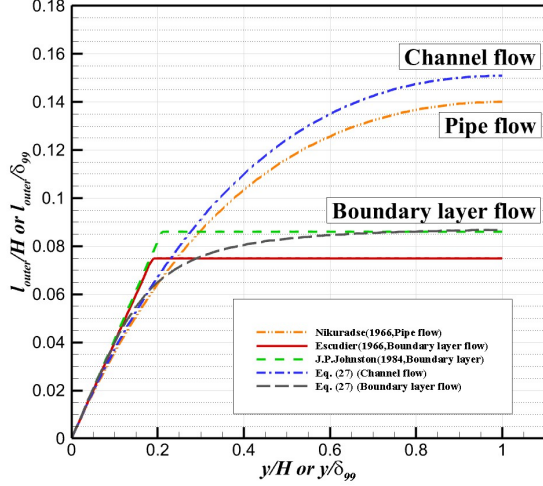


Figure 3: l_{outer} in different flow

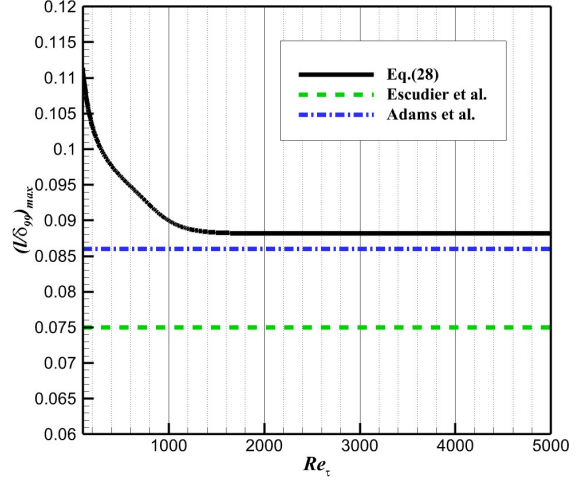


Figure 4: the maximum value of mixing length in Boundary layer flow

regression approach . For the channel flow, the mixing length in the outer region is significantly larger than for the boundary layer flow due to the absence of intermittent, which again seems to be in agreement with the current literature [Monty et al., 2007], where the outer-layer eddies are found to be smaller in the boundary layers and larger in channels, based on Prandtl's physical interpretation of the mixing length. In Fig.3,it is known that the mixing length monotonically increases within the boundary layer, and so the mixing length takes a maximum value at the edge of boundary layers.

$$\left(\frac{l}{\delta_{99}}\right)_{max} = \kappa \frac{\delta_{99}}{\delta_{99}} \tanh(l_k \left(\frac{\delta_{99}}{\delta_{99}}\right)^{-1}) \approx \kappa l_k \quad (28)$$

So , 0.215 is the maximum value of the mixing length at high Reynolds number divided by the Karmen constant.

Plotted in Fig.4,Eq.(28) gives the trend of the maximum values of mixing length at low Reynolds numbers, and in the next part, it can be found that because of capturing the law of change of mixing lengths at low Reynolds numbers, the simple formula plays an excellent role in numerical simulation with almost the same results as the direct numerical simulation(DNS).

4 Assessment and analysis

We have carried out the physical analysis of the mixing length formula, but how it can be used for the simulation of complex flows to construct a highly accurate turbulence model for engineering becomes significant.

At present, since the flow condition in engineering is basically high Reynolds number flow, the RANS method is still the main method In the RANS framework,the unclosed quantity-Reynolds stresses, are modeled using the turbulence model.So the predictive results are the best indicator of the turbulence model.

In the calculation process,We use the same boundary layer thickness determination method as Baldwin et al. [Baldwin and Lomax, 1978]

$$\delta_{99} = \frac{1}{0.65} \operatorname{argmax}(l|\Omega|) \quad (29)$$

where, $|\Omega|$ is the vorticity magnitude. And the eddy viscosity can be calculated by Eq.(30).

$$\nu_t = l^2 |\Omega| \quad (30)$$

This model is called Mixing Length symbolic regression(MLsr),Summarized in Fig.5.

4.1 Case1:Fully developed Channel(FDC)

The fully developed channel flow is described in Step . We use MLsr to predict the remaining three sets of flow condition($Re_\tau = 180, 550, 2000$) The predicted Reynolds stresses and velocity profiles are shown in Fig.6 and Fig.7. The prediction results show that both the velocity profiles and the Reynolds stresses predicted by MLsr are highly

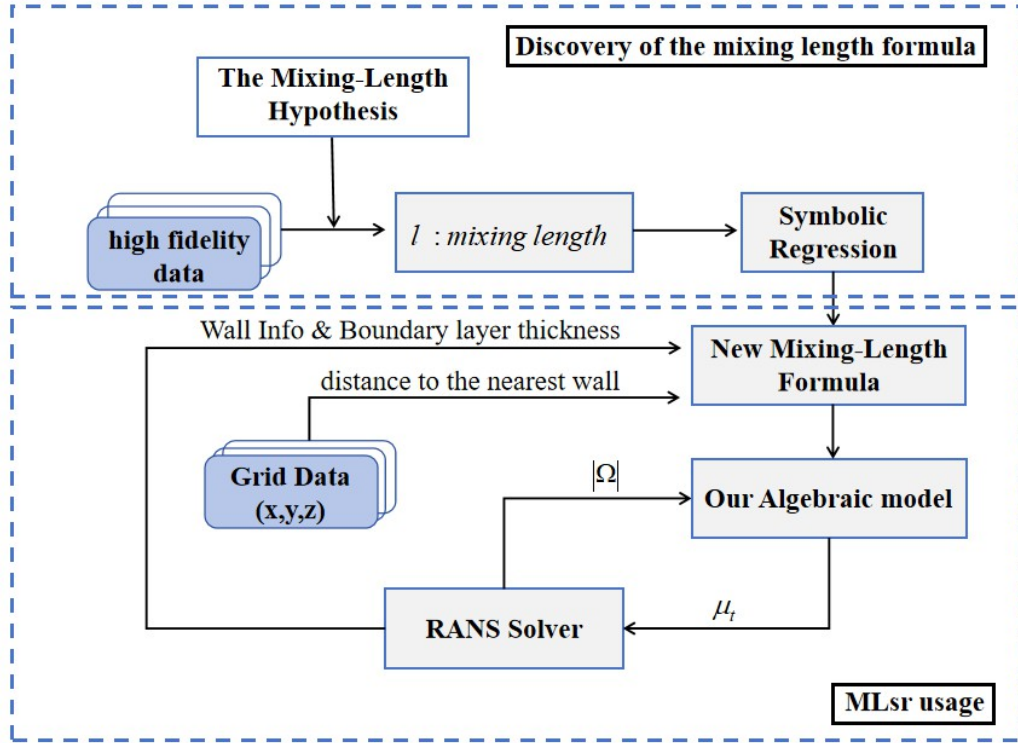


Figure 5: Discovery and usage

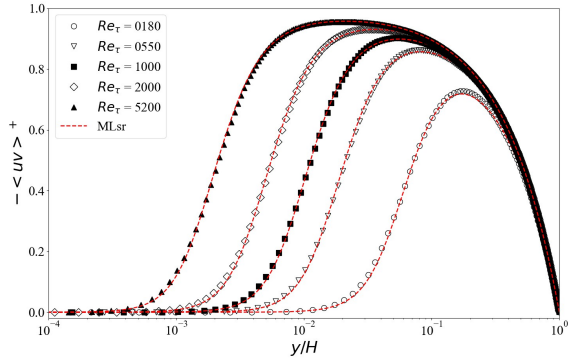


Figure 6: Reynolds stresses

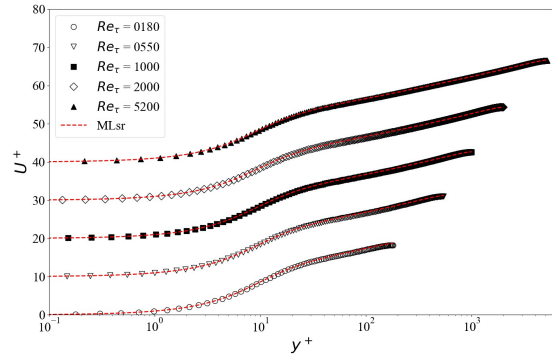


Figure 7: Velocity profiles

close to the DNS data. Based on the excellent results, we draw a conclusion that SR method mines the real physical laws from data and results prove its validation in the low friction Reynolds number flow, even though the data used for training is only a portion of the flow field data of two high friction Reynolds numbers (1000, 5200). This example strongly proves that mining physics formulas from data is not nonsense. And after the discovery of the effective physical formulas, it provides a theoretical approach for the further theoretical study of the flow mechanism of wall turbulence.

4.2 Case2: Zero Pressure Gradient Flat Plate Boundary Layer (ZPGFPBL)

This example is incompressible flow, and the boundary conditions are said in Step2

Fig.8 plots the surface friction coefficient as a function of Re_θ , which is the momentum loss thickness based Reynolds number. By observing Fig.8, it is obvious that at low momentum thickness Reynolds number, the DNS [Schlatter and Örlü, 2010], LES and RANS data all show deviations, but DNS is the most accurate numerical simulation method without no models involved. Surprisingly, the results predicted by MLsr are highly close to the DNS results at low momentum thickness Reynolds number. If we set $l_k = 0.215$ then the MLsr model without

considering the low Reynolds number effect predicts the same results as SST and SA at low Reynolds number, which also reflects that the low Reynolds number effect does not seem to be taken into account in the modeling of these two models.

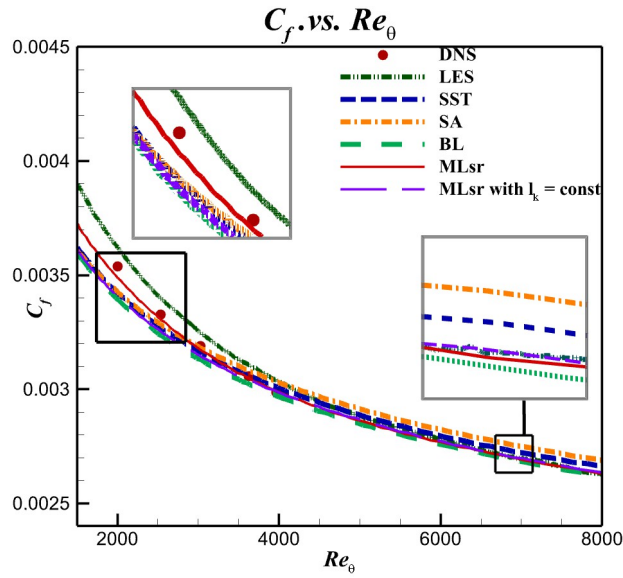


Figure 8: $C_f - Re_\theta$ in ZPGFPBL

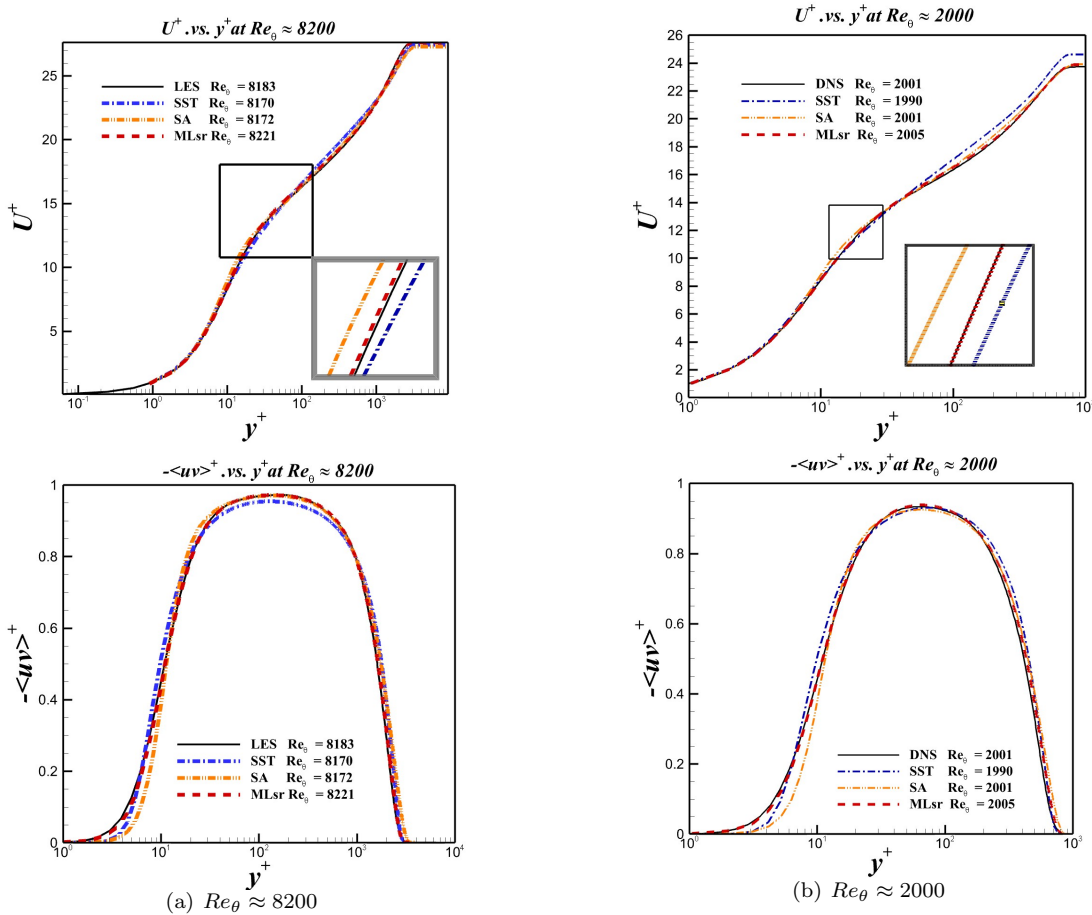


Figure 9: Two sections in ZPGFPBL

From Fig.?? , it can be seen that MLsr model outperforms the currently commonly used SST and SA models in both velocity profiles and Reynolds stress distributions. In particular, In viscous sublayer and buffer layer, MLsr model predicts significantly better Reynolds stress distributions than other turbulence models.It is not only because MLsr model is mined from high fidelity data, but also because the correct asymptotic relationship is found, which is commonly established in wall turbulence. Moreover, as can be seen, at low momentum thickness Reynolds number, the prediction results of MLsr are highly consistent with DNS results. Through the prediction results of the flat plate boundary layer flows, both at high momentum thickness Reynolds number and low momentum thickness Reynolds number, MLsr is much better than the existing turbulence models, and the inner function of mixing length formula is learned from channel flows, and the outer function is adapted according to the boundary conditions of the flow, but the prediction results show that the inner function is found to be adapted to two different types of wall-bounded flows, reflecting the consistent effect of the wall on the wall-bounded turbulence. We are once again firmly convinced that the mixing length formulas learned from the data captures the true physics of wall-bounded turbulence.

4.3 Case3:Incompressible flow over airfoil

Airfoils are the basic elements in the design of airplane wings, tail fins, missile airfoils, helicopter rotors, propellers, and wind turbine blades, which directly affect the aerodynamic performance of aerospace vehicles, so the prediction of airfoil flow is extremely crucial. Next, the famous subsonic airfoil NACA0012(Fig) will be used to verify the prediction capability and accuracy of MLsr.

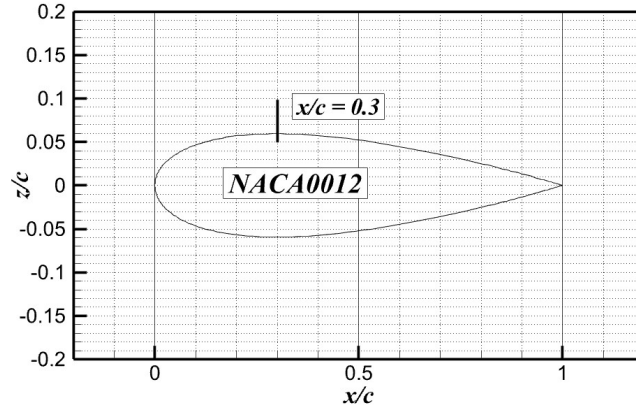


Figure 10: NACA0012

The flow field of the NACA0012 airfoil(see Fig.10) with a Reynolds number of 400,000 is computed at an angle of attack of 0 degrees using different turbulence models, and the results predicted by the different models were compared with data of the well-resolved LES [Tanarro et al., 2020]. This large eddy simulation accurately resolves the large-scale turbulence, while the smallest scales are modeled with the SubGrid stress model [Schlatter et al., 2004]. In Fig.11, MLsr predicts the surface friction stress distribution closest to the LES data, which is better than other models. Moreover, in this low Reynolds number case, the SST model and SA model results have large errors with the LES results, which seems to prove again the conclusion obtained from Case2 that these two models are not applicable to low Reynolds number flows. Meanwhile, we also performed the simulations before and after the removal of the γ function as a correction for the pressure gradient, and as we expected, the results deteriorated to some extent after the removal. In Fig.12, it is found that the pressure gradient correction only performed in the range ($y^+ < 50$) is able to trend consistently closer to the LES results for the whole cross section.

5 Conclusions

In the field of AI4Science research, symbolic AI has the potential to make a resurgence as a mainstream approach alongside connectionism. Symbolic AI, which focuses on the manipulation of symbols and rules to represent knowledge and perform reasoning tasks, offers unique advantages such as interpretability, transparency, and explicit representation of domain knowledge. By leveraging symbolic AI techniques in scientific applications, researchers may be able to better understand and explain the processes and decisions made by AI systems, leading to more

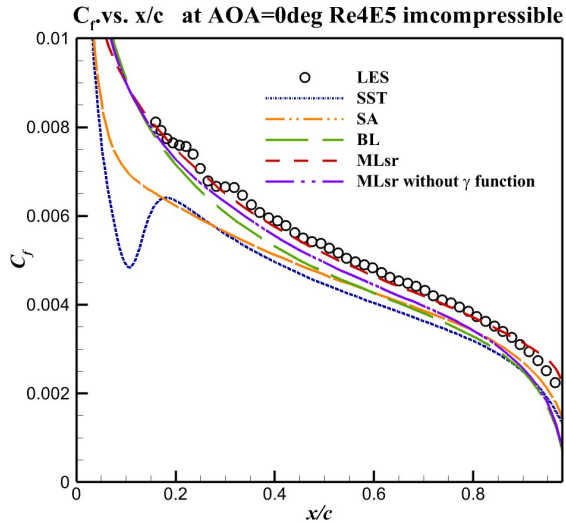


Figure 11: $C_f - x/c$

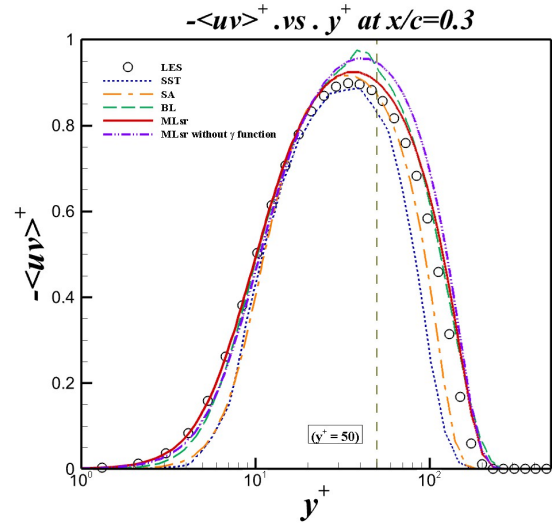


Figure 12: $-\langle uv \rangle^+ - y^+(x/c = 0.3)$

reliable and trustworthy results. With the increasing demand for explainable AI in scientific research, symbolic AI could play a key role in unlocking new insights and advancing the state of the art in AI4Science. In this research, we have made useful attempts in the field of turbulence.

In this paper, we mine mixing length formulas from DNS and LES data based on the mixing length hypothesis. In the process of mining physical formulas using symbolic regression, a three-step strategy is used creatively to fully mine high fidelity mixing length formulas. First, the basic forms of the mixing length are discovered directly from the data of the channel flow. For boundary layer flow, the effect of intermittency on the mixing length is taken into account, so we again learn the outer function for boundary layers flow from the data of the flat plate boundary layer. Thirdly, in addition to the generality of the existence of pressure gradients, their effects are also elusive. We thus learned pressure gradient corrections only at locations ($y^+ < 50$) where this effectively avoids the complexities of history effects. Coupled with RANS solver, the mixing length formula is used to predict channel flow, flat plate boundary layer flow, and airfoil flow. The results fully demonstrate the prediction accuracy of the formula. In the results of NACA0012, we are surprised to find that the prediction of C_f is really close to the LES results after the pressure gradient correction is applied to the mixing length, which is a strong example to tell us that the influence of complex factors such as history effects seems to have little effect on the prediction of surface friction stresses. The formula is simple enough that it is very easy to embed into the CFD code. However, simplicity is also a disadvantage in that it does not reflect the non-local nature of turbulence, and in the future we can try to bring it directly into the framework of wall-modelled large eddy simulations to serve as a high-precision wall model.

References

- [Adams and Johnston, 1984] Adams, E. and Johnston, J. (1984). A mixing-length model for the prediction of convex curvature effects on turbulent boundary layers.
- [Anderson and Wendt, 1995] Anderson, J. D. and Wendt, J. (1995). *Computational fluid dynamics*, volume 206. Springer.
- [Baldwin and Lomax, 1978] Baldwin, B. and Lomax, H. (1978). Thin-layer approximation and algebraic model for separated turbulent flows. In *16th aerospace sciences meeting*, page 257.
- [Bobke et al., 2017] Bobke, A., Vinuesa, R., Örlü, R., and Schlatter, P. (2017). History effects and near equilibrium in adverse-pressure-gradient turbulent boundary layers. *Journal of Fluid Mechanics*, 820:667–692.
- [Bobke et al.,] Bobke, A., Vinuesa, R., Örlü, R., and Schlatter, P. Large-eddy simulations of adverse pressure gradient turbulent boundary layers. In *Journal of Physics: Conference Series*, volume 708, page 012012. IOP Publishing. APG data.

- [Cebeci and Bradshaw, 2013] Cebeci, T. and Bradshaw, P. (2013). *Physical and computational aspects of convective heat transfer*. Springer Science & Business Media.
- [Chen et al., 2018] Chen, X., Hussain, F., and She, Z.-S. (2018). Quantifying wall turbulence via a symmetry approach. part 2. reynolds stresses. *Journal of Fluid Mechanics*, 850:401–438.
- [Cheng et al., 2018] Cheng, Y., Chen, K., Sun, H., Zhang, Y., and Tao, F. (2018). Data and knowledge mining with big data towards smart production. *Journal of Industrial Information Integration*, 9:1–13.
- [Clauser, 1956] Clauser, F. H. (1956). The turbulent boundary layer. *Advances in applied mechanics*, 4:1–51.
- [Cranmer, 2023] Cranmer, M. (2023). Interpretable machine learning for science with pysr and symbolicregression. jl. *arXiv preprint arXiv:2305.01582*.
- [Cui and Athey, 2022] Cui, P. and Athey, S. (2022). Stable learning establishes some common ground between causal inference and machine learning. *Nature Machine Intelligence*, 4(2):110–115.
- [de França et al., 2023] de França, F. O., Virgolin, M., Kommenda, M., Majumder, M., Cranmer, M., Espada, G., Ingelse, L., Fonseca, A., Landajuera, M., and Petersen, B. (2023). Interpretable symbolic regression for data science: Analysis of the 2022 competition. *arXiv preprint arXiv:2304.01117*.
- [Eitel-Amor et al., 2014] Eitel-Amor, G., Örlü, R., and Schlatter, P. (2014). Simulation and validation of a spatially evolving turbulent boundary layer up to $re_\theta = 8300$. *International Journal of Heat and Fluid Flow*, 47:57–69.
- [Escudier and Spalding, 1966] Escudier, M. and Spalding, D. B. (1966). A note on the turbulent uniform-property hydrodynamic boundary layer on a smooth impermeable wall comparisons of theory with experiment.
- [Gungor et al., 2016] Gungor, A. G., Maciel, Y., Simens, M., and Soria, J. (2016). Scaling and statistics of large-defect adverse pressure gradient turbulent boundary layers. *International Journal of Heat and Fluid Flow*, 59:109–124.
- [Hey et al., 2009] Hey, T., Tansley, S., Tolle, K. M., et al. (2009). *The fourth paradigm: data-intensive scientific discovery*, volume 1. Microsoft research Redmond, WA.
- [Klebanoff, 1955] Klebanoff, P. S. (1955). Characteristics of turbulence in boundary layer with zero pressure gradient. Technical report.
- [Lee and Moser, 2015] Lee, M. and Moser, R. D. (2015). Direct numerical simulation of turbulent channel flow up to. *Journal of fluid mechanics*, 774:395–415.
- [Ling et al., 2016] Ling, J., Kurzawski, A., and Templeton, J. (2016). Reynolds averaged turbulence modelling using deep neural networks with embedded invariance. *Journal of Fluid Mechanics*, 807:155–166.
- [Matchev et al., 2022] Matchev, K. T., Matcheva, K., and Roman, A. (2022). Analytical modeling of exoplanet transit spectroscopy with dimensional analysis and symbolic regression. *The Astrophysical Journal*, 930(1):33.
- [Mellor and Gibson, 1966] Mellor, G. and Gibson, D. (1966). Equilibrium turbulent boundary layers. *Journal of Fluid Mechanics*, 24(2):225–253.
- [Monty et al., 2007] Monty, J., Stewart, J., Williams, R., and Chong, M. (2007). Large-scale features in turbulent pipe and channel flows. *Journal of Fluid Mechanics*, 589:147–156.
- [Murata et al., 2020] Murata, T., Fukami, K., and Fukagata, K. (2020). Nonlinear mode decomposition with convolutional neural networks for fluid dynamics. *Journal of Fluid Mechanics*, 882:A13.
- [Park and Choi, 2021] Park, J. and Choi, H. (2021). Toward neural-network-based large eddy simulation: Application to turbulent channel flow. *Journal of Fluid Mechanics*, 914:A16.
- [Pirozzoli, 2014] Pirozzoli, S. (2014). Revisiting the mixing-length hypothesis in the outer part of turbulent wall layers: mean flow and wall friction. *Journal of fluid mechanics*, 745:378–397.
- [Prandtl, 1925] Prandtl, L. (1925). Über die ausgebildete turbulenz (investigations on turbulent flow). *Z. Angew. Math. Mech*, 5:136–139.

- [Reynolds, 1895] Reynolds, O. (1895). Iv. on the dynamical theory of incompressible viscous fluids and the determination of the criterion. *Philosophical transactions of the royal society of london.(a.)*, (186):123–164.
- [Schlatter and Örlü, 2010] Schlatter, P. and Örlü, R. (2010). Assessment of direct numerical simulation data of turbulent boundary layers. *Journal of Fluid Mechanics*, 659:116–126.
- [Schlatter et al., 2004] Schlatter, P., Stolz, S., and Kleiser, L. (2004). Les of transitional flows using the approximate deconvolution model. *International journal of heat and fluid flow*, 25(3):549–558.
- [Shan et al., 2023] Shan, X., Liu, Y., Cao, W., Sun, X., and Zhang, W. (2023). Turbulence modeling via data assimilation and machine learning for separated flows over airfoils. *AIAA Journal*, 61(9):3883–3899.
- [Tanarro et al., 2020] Tanarro, Á., Vinuesa, R., and Schlatter, P. (2020). Effect of adverse pressure gradients on turbulent wing boundary layers. *Journal of Fluid Mechanics*, 883:A8.
- [Townsend, 1956] Townsend, A. (1956). The properties of equilibrium boundary layers. *Journal of Fluid Mechanics*, 1(6):561–573.
- [Townsend, 1961] Townsend, A. (1961). Equilibrium layers and wall turbulence. *Journal of Fluid Mechanics*, 11(1):97–120.
- [Van Driest, 1956] Van Driest, E. R. (1956). On turbulent flow near a wall. *Journal of the aeronautical sciences*, 23(11):1007–1011.
- [Wadekar et al., 2023] Wadekar, D., Thiele, L., Hill, J. C., Pandey, S., Villaescusa-Navarro, F., Spergel, D. N., Cranmer, M., Nagai, D., Anglés-Alcázar, D., and Ho, S. (2023). The sz flux-mass (y - m) relation at low-halo masses: improvements with symbolic regression and strong constraints on baryonic feedback. *Monthly Notices of the Royal Astronomical Society*, 522(2):2628–2643.
- [Wang et al., 2019] Wang, Y., Wagner, N., and Rondinelli, J. M. (2019). Symbolic regression in materials science. *MRS Communications*, 9(3):793–805.
- [Wu and Zhang, 2023] Wu, C. and Zhang, Y. (2023). Enhancing the shear-stress-transport turbulence model with symbolic regression: A generalizable and interpretable data-driven approach. *Physical Review Fluids*, 8(8):084604.
- [Wu et al., 2013] Wu, Y., Chen, X., She, Z.-S., and Hussain, F. (2013). On the karman constant in turbulent channel flow. *Physica Scripta*, 2013(T155):014009.
- [Xu et al., 2023] Xu, D., Wang, J., Yu, C., and Chen, S. (2023). Artificial-neural-network-based nonlinear algebraic models for large-eddy simulation of compressible wall-bounded turbulence. *Journal of Fluid Mechanics*, 960:A4.
- [Zhang and Ma, 2020] Zhang, J. and Ma, W. (2020). Data-driven discovery of governing equations for fluid dynamics based on molecular simulation. *Journal of Fluid Mechanics*, 892:A5.
- [Zhou et al., 2020] Zhou, Y., Fan, D., Zhang, B., Li, R., and Noack, B. R. (2020). Artificial intelligence control of a turbulent jet. *Journal of Fluid Mechanics*, 897:A27.
- [Zhu et al., 2021] Zhu, L., Zhang, W., Sun, X., Liu, Y., and Yuan, X. (2021). Turbulence closure for high reynolds number airfoil flows by deep neural networks. *Aerospace Science and Technology*, 110:106452.